TCM Analysis of Defected Ground Structures for MIMO Antenna Designs in Mobile Terminals

ASIM GHALIB AND MOHAMMAD S. SHARAWI, (Senior Member, IEEE)
Electrical Engineering Department, King Fahd University for Petroleum and Minerals, Dhahran 31261, Saudi Arabia

Corresponding author: Mohammad S. Sharawi (msharawi@kfupm.edu.sa)

ABSTRACT In this paper, the theory of characteristic modes (TCMs) is used for the first time to analyze the behavior of defected ground structures (DGS), when added to antenna designs. A properly designed DGS introduces currents opposite in direction to the original characteristic modes (CM) currents thus reducing mutual coupling. TCM is also applied to multiple-input-multiple-output (MIMO) antenna systems to develop a systematic approach that can predict whether the isolation can be enhanced further or not. For this purpose two 4-element and one 2-element MIMO designs, i.e. monopole and planar inverted-F antennas are studied. The addition of different antenna elements affects the CM significantly as well as differently. Some of the CM excited on the antenna surface contributes to the coupling between the antenna ports that is why they can be classified as coupling modes. To improve the isolation, the DGS should be introduced at certain locations that blocks the coupling modes but at the same time does not affect the non-coupling modes. If there is no such location or the current on the surface of the chassis for coupling and non-coupling modes is approximately same, the isolation cannot be enhanced further. Using this approach, isolation was improved on an average by 11 dB in all the designs considered, giving the most isolation enhancement following a systematic way compared to other works.

INDEX TERMS Theory of characteristic modes (TCM), defected ground structures (DGS), multiple-input-multiple-output (MIMO), isolation, planar inverted-F antenna (PIFA), chassis-mode antennas.

I. INTRODUCTION

High data rates in current and future generations of wireless terminals (without increasing the frequency or power levels) can be achieved by installing multiple antennas at the base station and terminal sides. The compactness of the terminals may degrade the performance of multiple-input-multiple-output (MIMO) systems due to high port and field coupling which affect the channel capacity, bandwidth (BW) and efficiency of the system [1]. Many methods are proposed in literature to improve port isolation with minimal effect on the channel capacity, BW and efficiency of the system. Isolation can be improved by the use of electromagnetic band-gap structures and meta-surfaces [2]–[4], decoupling networks [5], neutralization line technique [6], [7], parasitic elements [8], [9], optimization of the antenna system configuration [10], [11], introducing planar modified mushroom structures [12], [13] and the use of defected ground structures (DGS) [14]–[24]. Among all the aforementioned port isolation enhancement methods, DGS is the least complex and expensive.

Several DGS shapes were used between 2 and sometimes 4-element MIMO antenna systems to improve isolation such as using periodic S-shapes [14], T-shapes and slot lines [15], rectangular rings and slots [16], [17], ground (GND) slits [18]–[22] and arcs [23], [24]. The main problem in the DGS method for enhancing isolation is determining its shape, size and position along with the large amount of optimization time involved, and until now, no systematic design method is available.

The theory of characteristic modes (TCM) was developed in [25] and later modified by diagonalizing the impedance matrix in [26]. Characteristic modes (CM) are the real modes of the geometry that obey

$$[X]J_n = \lambda_n[R]J_n \tag{1}$$

where R and X represents the real and imaginary parts of the impedance operator (Z), λ_n is the eigen value corresponding to the current density eigen vector J_n [27]. The orthogonal behavior and linear independence of the CM are of great importance. The total current density (J) on the surface of

an antenna is the linear weighted sum with coefficients α_n of its CM currents.

$$J = \sum_n \alpha_n J_n \qquad (2)$$

where

$$\alpha_n = \frac{V_n^i}{1 + j\lambda_n} \qquad (3)$$

and V_n^i describes the effect of external excitation on a specific CM.

To obtain pattern reconfigurability, single modes are to be excited [27], [28]. A weighted sum of the modes can be of use as well. Multiple techniques were proposed to excite such single modes like using multiple sources [27], meandering or beveling or the addition of metallic strips to the antenna geometry to support the excitation of a single mode [28], [29], and using capacitive coupled elements (CCE) [30] or inductive coupled elements (ICE) [31], [32].

For frequencies below 1 GHz, the chassis (GND plane) acts as the main radiator. That is why severe coupling is observed in MIMO configurations because all antennas are coupled via the chassis. From TCM analysis, the first mode has electric field maximas at the edges of the chassis, while minimas are at the center. Any electrical antenna located at the edge will excite the chassis effectively while those located at the center will not. For a monopole located at the edge and a planar inverted-F antenna (PIFA) located at the center an isolation enhancement of 5 dB was achieved without using any isolation scheme as compared to placing them at the edges of the chassis [33]. The placement of the antenna at the center of the chassis is impractical, that is why it was observed that instead of placing two electrical antennas at the edges of the chassis, an electric and magnetic ones will have better isolation. At the edge, the magnetic fields have minimas that is why electric and magnetic antennas placed at the edge will have better isolation [34]. In [33] and [34] only the behavior of the first mode using TCM was examined and the analysis were based on it and no DGS behavior was investigated.

In this work, for the first time we will use TCM to analyze the behavior of a DGS in order to give an insight into the physical phenomena of isolation enhancement in MIMO antennas and to develop a systematic approach that can predict whether a DGS for a particular design can enhance the isolation or not. Our major contributions in this work are:

- Using TCM, an explanation to the physical behavior of DGS is provided. CM current distribution and modal significance (MS) curves are used for the comparison of modes. All modes present in the impedance BW region are considered for comparison while previously in [33], [34] the comparison was performed only for one mode. In addition the DGS behavior or its placement were not investigated before.
- To develop a systematic approach that can predict whether a DGS can enhance the isolation between

MIMO antenna elements or not. We consider three real antenna designs from the literature with different element types and characteristic (i.e. PIFA and monopole like) while previous works focused on chassis modes and their excitation.

- An average of 11 dB of isolation enhancement is achieved in three different designs considered.
- The effect of small antenna elements on the chassis modes is also investigated. It is observed that different antenna types affect the CM and MS differently which is usually overlooked in literature.
- For the first time, we compare the real/total currents on the surface of antennas with the CM currents and it is verified that real currents are approximately the weighted sum of the modal currents, which means that it is difficult to have isolated modes excited with real antenna elements. In the presence of real antenna elements, the chassis modes are significantly affected and we cannot rely only on the CM of the chassis.
- The two printed designs investigated include the effect of the dielectric substrate when TCM was performed.

The rest of the paper is organized as follows. Sections II describes the antenna designs and their analysis using TCM. Section III describes the behavior of DGS as well as discusses the method developed for isolation enhancement. MIMO antenna parameters are analyzed in section IV, while in section V the paper is concluded.

II. ANTENNA DESIGN AND ANALYSIS CASES

For the analysis purposes of the DGS using TCM, we have considered one wire [20] and two printed [22], [23] based MIMO antenna designs of different types: PIFA and monopole. Performing the analysis on different designs will help us in generalizing our findings. For a fair comparison, the chassis size is the same for the printed antenna designs, that is 100×60 mm^2, also the targeted BW is 150 MHz ($2.15 - 2.33$ GHz).

TCM analysis was performed with a series of cases, starting from a rectangular chassis representing the GND plane of a standard smart phone, chassis with a single cut (the cut below the antenna), chassis with double cuts and four cuts in the ground plane (for 2 and 4-element MIMO designs), chassis with a single antenna, 2-element MIMO connected along the width and then along the length of the chassis and finally the 4-element MIMO design. The isolation between the antennas was enhanced by properly studying the modal behavior. First, modes were identified in the desired band of interest and then a DGS was placed to block the modes that were causing high coupling. After the placement of the DGS, the antennas were again analyzed using TCM and we observed that the modes (causing high coupling) were not contributing in the desired BW of interest.

To be brief, we will present the main cases from our TCM analysis which are: the rectangular chassis, 4-element PIFA and Monopole based MIMO designs as well as the

cases when the DGS was introduced. All the analysis was conducted using CST electromagnetics package.

Since the chassis is the same in both designs, the CM current distributions at 2.2 GHz on its surface as well as the MS curves for the first 6-modes on the rectangular chassis are plotted in Figures 1 and 2, respectively. Figure 1 shows the modes on the chassis, where high currents are marked with big red arrows. The MS is an important figure of merit that represents the normalized amplitude of current modes and determines the radiation performance of modes. It depends on the size and shape of the object. The range of frequencies for which the power radiated is not less than one half the power radiated by the mode at resonance is known as the radiating BW and it is marked by the 0.707 point on the MS curves [27]. The impedance BW is calculated in the presence of the excitation sources and is the range of frequencies for which the antenna has good impedance matching (VSWR<2.0). Only 4 modes (1-4) are contributing in the desired impedance BW. These modes are the ones that we will compare against in the analysis to come.
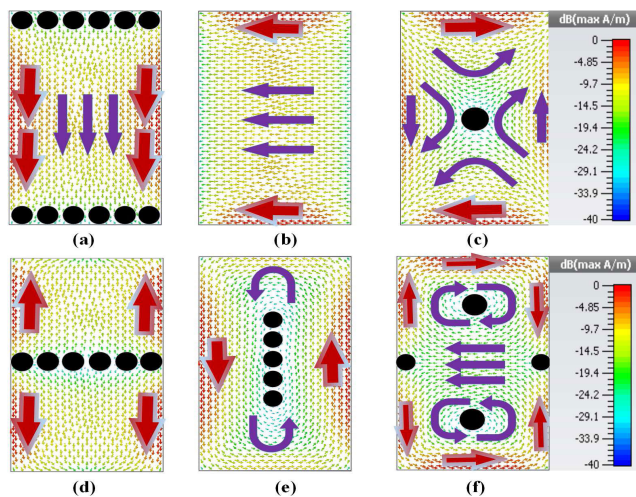

FIGURE 2. Modal Significance curves of the ground plane or chassis.

FIGURE 1. Current distribution of the first six modes of the chassis in the presence of an FR-4 substrate at 2.20 GHz, where (a) mode 1 (b) mode 2 (c) mode 3 (d) mode 4 (e) mode 5 (f) mode 6. Red arrows show the location as well as the direction of the maximum current of a mode. The black dots show the current null or current minima location while the violet arrows represent the current distribution on the surface of the chassis.

A. PIFA BASED 4-ELEMENT MIMO ANTENNA DESIGN

The geometry of the 4-element MIMO PIFA like design is shown in Figures 3(a) and 3(b). The antenna was designed on an FR4 substrate with a relative permittivity (ϵ_r) of 4.0, loss tangent of 0.02 and thickness of 0.8 mm. The total design area was 100×60 mm^2. Figure 3(c) shows the top view of the fabricated design containing the 4-elements PIFA like MIMO antenna system while Figure 3(d) shows the bottom layer containing the ground for all the antenna elements. The 3D view of the PIFA is shown in the Figure 4(a), where SP represents the shorting post. Three prototypes were made, without DGS, with one DGS and
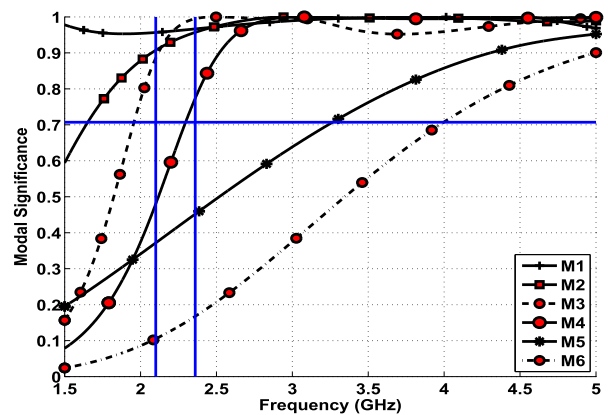
with 2 DGS structures. Only the final prototype is shown for brevity.

The fabrication, development of the antenna prototype and port measurements were performed at the Antennas and Microwave Structure Design Lab (AMSDL) at King Fahd University of Petroleum and Minerals (KFUPM) using an LPKF S103 machine and an Agilent N9918A Vector Network Analyzer (VNA). The gain patterns and efficiencies were measured using a SATIMO Starlab anechoic chamber at Microwave Vision Group (MVG), Italy.

The measured impedance BW (VSWR<2,-10 dB) of the design without DGS slots was 180 MHz ranging from 2.153 to 2.333 GHz (Figure 3(e)) while a measured isolation of 16.25 dB was achieved between Ant-1 and Ant-3 as shown in Figure 3(f). To improve the performance of the system we need to enhance the isolation.

TCM was applied to the 4-element PIFA like MIMO design including its substrate as shown in Figure 3. The modal current distribution on the surface of the chassis at 2.2 GHz and the MS curves are shown in Figures 5 and 6, respectively. One can clearly observe from Figures 5 and 6 that it is not only the chassis that decides the CM behavior. If we observe the current distribution we can see that the current maximas are now shifted towards the antenna elements, but the general pattern of chassis modes are not affected significantly except modes 1 and 4 where the null position has shifted. The CM current distribution was significantly reduced on the chassis that is why we showed it on a 50 dB scale. The current reduction on the chassis and the shifting of the current maxima to the antenna elements shows that the antennas are playing a major role in the radiation mechanism. If we look at the MS curves, we observe that the addition of these antennas has significantly affected the modes in terms of the radiating BW as observed in Figure 6. The antennas have limited radiating BW of modes 1 and 3 to 3.2 GHz. Modes 2 and 4 start contributing to the radiating BW at around 2.18 GHz which is exactly the same point where our measured BW starts, this is an indication that one or both can be excited on the surface of the antenna by the real excitation/source.
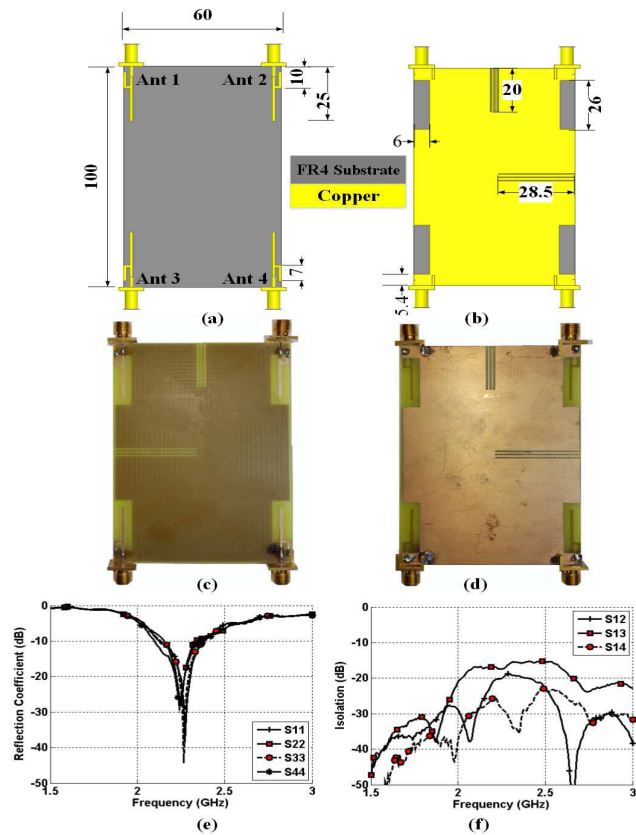
FIGURE 3. Geometry of the 4-element MIMO PIFA deisgn (a) top view, (b) bottom view with DGS, all dimensions are in mm (c) fabricated prototype top view, (d) fabricated prototype bottom view with DGS, (e) measured reflection coefficient without DGS, (f) measured isolation without DGS.
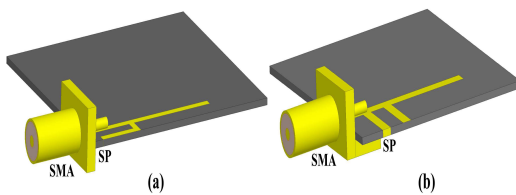

FIGURE 4. 3D view of single element (a) PIFA, (b) monopole.

B. MONOPOLE BASED 4-ELEMENT MIMO DESIGN

The geometry of the 4-element MIMO Monopole like design is shown in Figures 7(a) and 7(b). The 3D view of the Monopole is shown in the Figure 4(b), where SP represents the shorting post. The antenna was designed with the same substrate properties as the PIFA one. The fabricated prototype with the DGS is shown in Figures 7(c) and 7(d) for the top and bottom views respectively.

The measured impedance BW without the DGS was 165 MHz ranging from 2.085 to 2.25 GHz as shown in Figure 7(e), while the minimum measured isolation was 15.5 dB as shown in Figure 7(f) between Ant-1 and Ant-3. To improve the isolation we will use a DGS.

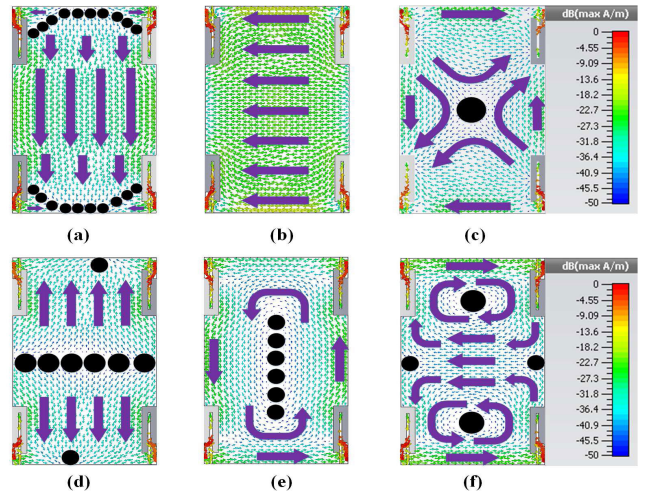Like the PIFA design, TCM was also applied to the 4-element MIMO Monopole like design including

FIGURE 5. Current distribution of the first six modes of the 4-element MIMO PIFA in the presence of an FR-4 substrate at 2.20 GHz, where (a) mode 1 (b) mode 2 (c) mode 3 (d) mode 4 (e) mode 5 (f) mode 6. The black dots show the current null or current minima location while the violet arrows represent the current distribution on the surface of chassis.
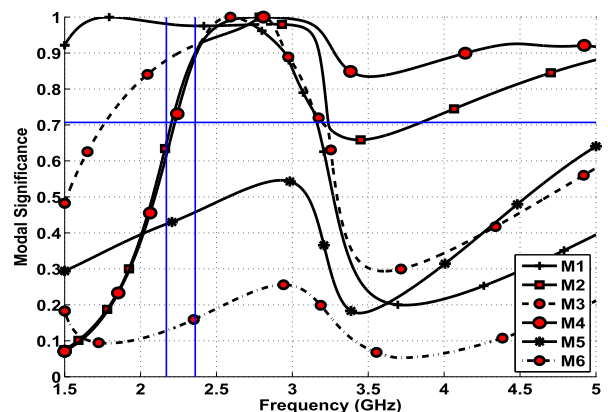

FIGURE 6. Modal significance curves of the 4-element PIFA based MIMO in the presence of the FR-4 substrate.

the substrate. The modal current distribution at 2.2 GHz and MS curves are shown in Figure 8 and 9, respectively. We can clearly observe that the antennas in both designs affected the CM and MS curves differently. This verifies that small antenna elements have a noticeable effect on the CM. For the 4-element MIMO Monopole like antenna system, the CM are affected except for mode 2 current distribution which seems to be totally unaffected. Mode 3 is severely affected and is no longer contributing to the radiating BW in the desired impedance BW of interest while mode 6 is contributing at lower frequencies. Mode 1 has now a limited radiating BW. Only modes 1 and 2 are contributing to the radiating BW in the desired impedance BW of interest.

III. DEFECTED GROUND STRUCTURE ANALYSIS
A. PIFA BASED MIMO DESIGN
We can observe from Figure 6 that modes 1, 2, 3 and 4 are contributing to the radiating BW in the desired impedance
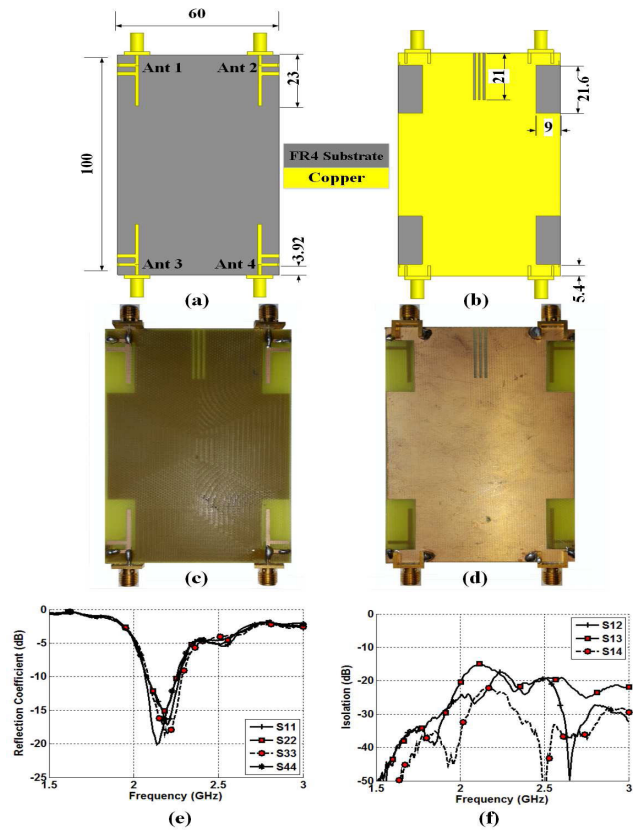
FIGURE 7. Geometry of the 4-element MIMO PIFA deisgn (a) top view, (b) bottom view with DGS, all dimensions are in mm (c) fabricated prototype top view, (d) fabricated prototype bottom view with DGS, (e) measured reflection coefficient without DGS, (f) measured isolation without DGS.
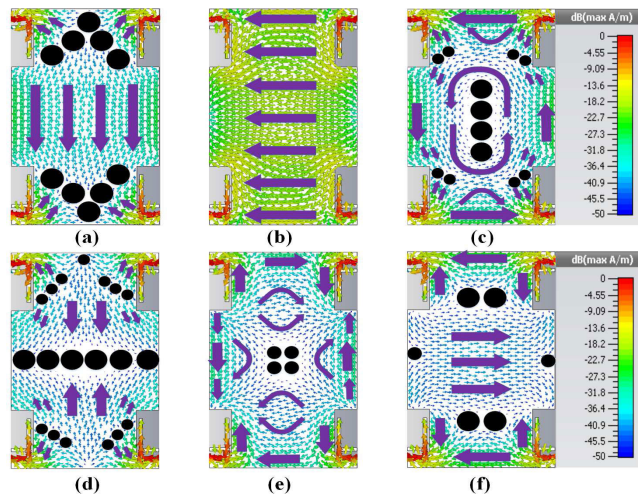

FIGURE 9. Modal significance curves of the 4-element MIMO monopole in the presence of FR-4 substrate.

FIGURE 10. Current distribution on the surface of the 4 element MIMO PIFA antenna at 2.2 GHz when all antenna's are excited (a) without any DGS, (b) DGS between Ant-1 and 3.

FIGURE 8. Current distribution of the first six modes of the 4-element MIMO monopole in the presence of an FR-4 substrate at 2.20 GHz, where (a) mode 1 (b) mode 2 (c) mode 3 (d) mode 4 (e) mode 5 (f) mode 6. The black dots show the current null or current minima location while the violet arrows represent the current distribution on the surface of chassis.

BW of interest while modes 5 and 6 are not contributing at all. Moreover based on the current directions, we can observe that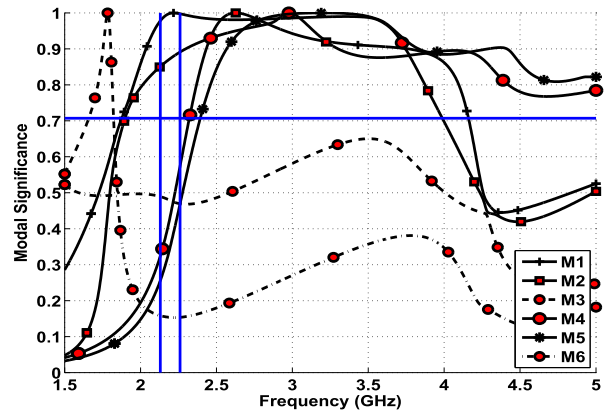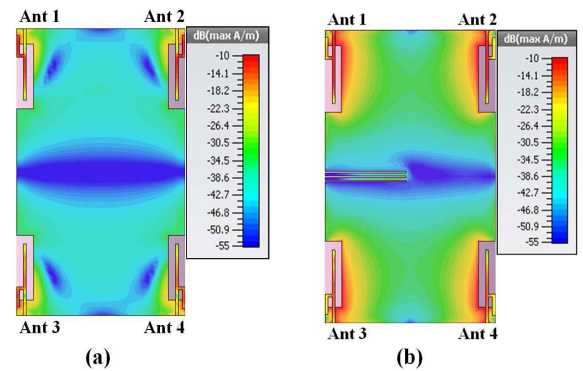 mode 1 is neither contributing to the coupling between the horizontal or vertical antennas (due to the presence of current nulls) while mode 3 is causing the coupling between the antennas connected on the longitudinal side (Ant1-Ant3) as well as the horizontal side (Ant1-Ant2) and modes 2 and 4 are causing the coupling between Ant-1 and Ant-2. Modes 2 and 4 are not contributing to the coupling between the Ant1 and Ant3.

The total current on the surface of the antenna and chassis is shown in Figure (10)(a). It can be clearly observed that the total current on the surface of the antenna seems to be the combination of modes 1 and 4 in particular, that is why we observe a current null (blue spot) near the antennas (representing mode 1 because other modes do not have such a null at this location) and in the middle of the chassis (representing mode 4 because other modes do not have such a null at this location) while modes 2 and 3 seem to be excited less effectively because mode 2 current is uniform (Figure 5(b)) and there is no uniformity in Figure (10)(a).

From the isolation plot shown in Figure 3(f) the isolation is worst between the antennas 1 and 3, so we need to improve it. The concept of placing the slots is simple and straight forward. The slot should be placed at a location such that it blocks the coupling modes, but at the same time it should not

affect or block the non-coupling modes. The idea is simple if we have two modes in the desired impedance BW where one is a coupling mode and the other is a non-coupling one and they can be separated where one can be blocked without affecting the other. But it gets complicated whenever we have to deal with more modes.

The only mode that is contributing to the coupling between Ant1 and Ant3 is mode 3. Mode 3 is behaving as a coupling mode so we need to block it in order to improve the isolation but at the same time we should be careful that the DGS to be introduced does not affect the non-coupling modes (mode 1 and 4) significantly. Both modes 1 and 4 have got different current distributions, so we need to place the DGS at a location with minimum non-coupling mode disturbance. There can be three possibilities, current null location of mode 4 (will not affect mode 4 but will affect mode 1), or mode 1 (will not affect mode 1 but will affect mode 4), or any other location (will affect modes 1 and 4) on the chassis. The current null location of mode 1 is very close to the edge of the chassis so placing any slot at this location will completely isolate the antennas and it will seem that the antennas are operating with different ground planes which is not acceptable. If we place the slot at any other location, it will affect both the non-coupling modes of mode 1 and 4 and it will severely affect the impedance BW. So, the optimum position to block mode 3 seems to be the current null location of mode 4 (which is at the middle of chassis), placing a DGS at this location will block mode 3 but will not affect modes 4 and 2, while mode 1 will be slightly affected. For mode 1, its radiating BW covers up to 3.2 GHz, so introducing a discontinuity in the current path will affect its radiating BW.

A DGS structure consisting of single slit line could not meet the criteria that is why a simple DGS structure consisting of three slit lines was chosen so that the concept can be proved and can be generalized to any design irrespective of its antenna type. In general, the width, length and inter-slot separation are optimized for a certain center frequency of interest. This will also help the designer to spend minimum time on optimization. The DGS was introduced in the center of the chassis between Ant 1 and 3 (Figure 3(b)). The total size of the DGS was 28.5×3.5 mm^2 with an arm length of 28.5 mm, slit width of 0.5 mm and slit separation of 1 mm.

Before showing the improvement in S-parameters, let us discuss how the DGS affects the CM. The CM current distribution at 2.2 GHz and the MS plots are shown in Figures 11 and 12, respectively. Modes 2 and 4 current distributions are totally unaffected because the DGS structure is parallel to the current direction (mode 2) or its lying at the current null (mode 4). Modes 1 and 3 current patterns are affected. The DGS generates a current distribution that is opposite to the original current flow as shown in modes 1, 3 and 5, thus reducing the coupling between the antenna elements. The interesting part is that mode 3 is no longer contributing in the desired radiating BW of interest and is shifted to lower frequencies with very narrow radiating BW as shown in Figure 12. Mode 1 has greater
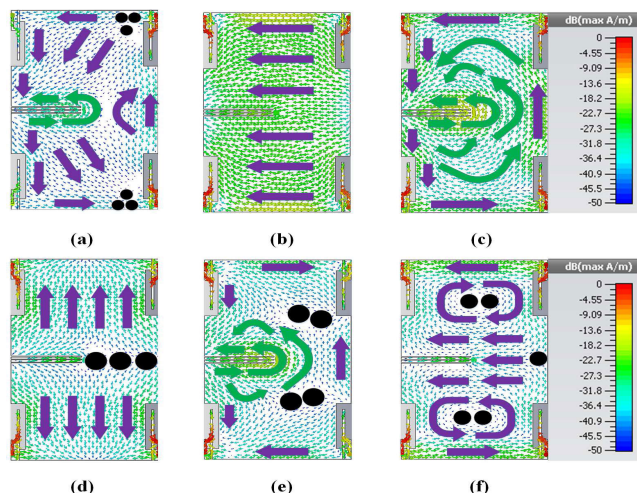

FIGURE 11. Current distribution of the first six modes of the 4-element PIFA like MIMO in the presence of the DGS at 2.20 GHz, where (a) mode 1 (b) mode 2 (c) mode 3 (d) mode 4 (e) mode 5 (f) mode 6. The green arrows show the current distribution created due to the introduction of DGS. The black dots show the current null or current minima location while the violet arrows represent the current distribution on the surface of chassis.
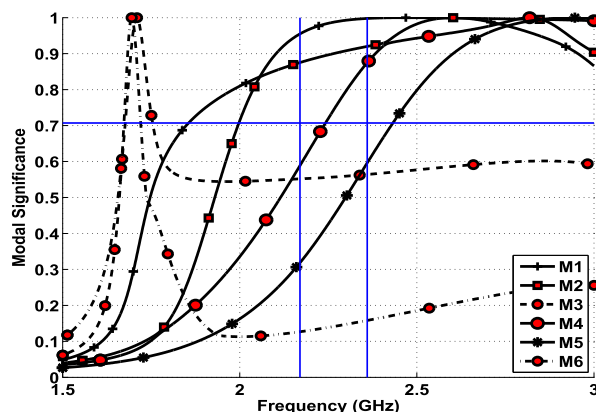

FIGURE 12. Modal significance curves of the 4-element PIFA like MIMO in the presence of DGS.

than 100 % radiating BW starting at 1.87 GHz. In the desired BW of interest, it is not affected. Mode 1 radiating BW was affected (compared to Figure 6) but in our BW of interest its not affected significantly. Modes 5 and 6 are also affected. Mode 6 radiating BW is shifted to lower frequencies while mode 5 is contributing to the radiating BW after 2.42 GHz. The isolation between the antenna elements was improved by 12.75 dB.

The second objective is to improve the isolation between the Ant1 and Ant2. Modes 1,2 and 4 are contributing to the radiating BW in the desired band as shown in Figure 12. Modes 2 and 4 seem to be contributing to the coupling between antennas 1 and 2. The total current on the surface of the antenna and chassis in the presence of the first DGS was shown in Figure (10)(b). It can be clearly observed that the addition of the DGS has confined the current

distribution more towards the antenna elements. The total current on the surface of the antenna and chassis seems to be the combination of modes 1 and 4. Mode 2 has uniform current distribution so it seems that either mode 2 is not excited or it is excited with minimum contribution. The only mode left that can cause the coupling seems to be the mode 4 as mode 1 has a current null between the antennas connected on the horizontal side.

If we place a DGS between Ant1 and Ant2 this will help us in separating the current direction of mode 4 as well as it will not affect the current distribution of mode 1 significantly. Again the simplest DGS structure consisting of three slit lines was chosen. After few parametric sweeps the DGS was tuned with a the total size of 20×3.1 mm^2 with an arm length of 20 mm, width of the slit is 0.7 mm and slit separation of 0.5 mm. The geometry of the proposed two DGS structures on the 4-element PIFA like MIMO design are shown in Figure 3(b), while Figure 3(d) shows the fabricated bottom layer containing the DGS on the ground.

The CM current distribution at 2.2 GHz and the MS plots are shown in Figure 13 and 14, respectively, for the design in Figure 3 with the two DGS structures. From the MS curves we can observe that only modes 1 and 2 are present in the radiating BW region while mode 4 is blocked in the desired band. We can conclude that either mode 1 or mode 2 or a combination of them are responsible for the radiation. The radiating BW of mode 1 and the impedance BW of the real design stops exactly at the same point, as shown in Figure 15, this means that mode 1 is playing a significant role. Modes 3, 5 and 6 are not contributing in the desired impedance BW of interest.
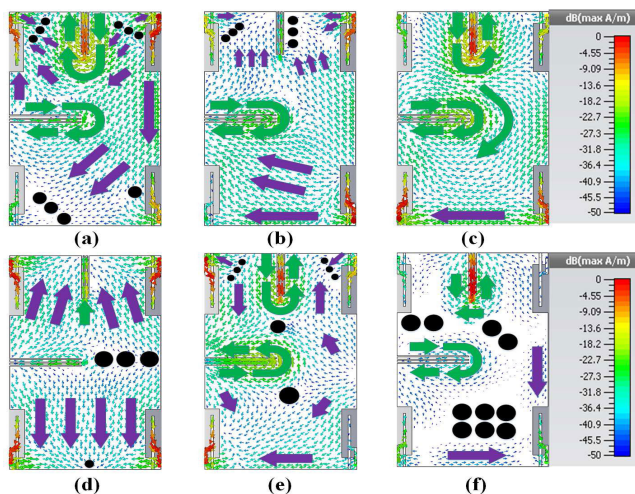

FIGURE 14. Modal significance curves of the 4-element MIMO in the presence of two DGS. The vertical blue lines represent the impedance BW.

FIGURE 15. 4-element PIFA design, (a) measured reflection coefficient with DGS, (b) measured isolation curve with DGS, (c) current distribution without DGS when Ant-1 is excited, (d) current distribution with DGS when Ant-1 is excited.

FIGURE 13. Current distribution of the first six modes of the 4-element MIMO PIFA in the presence of two DGS at 2.20 GHz, where (a) mode 1 (b) mode 2 (c) mode 3 (d) mode 4 (e) mode 5 (f) mode 6. The green arrows show the current distribution created due to the introduction of DGS. The black dots show the current null or current minima location while the violet arrows represent the current distribution on the surface of chassis.

The reflection coefficient and the isolation curves of the PIFA MIMO antenna with DGS is shown in Figure 15(a) and 15(b). We can observe that a measured
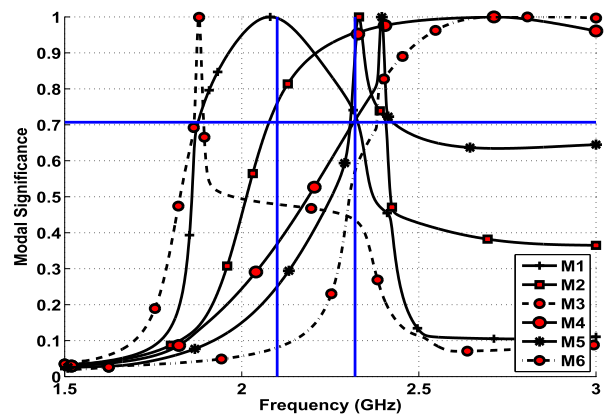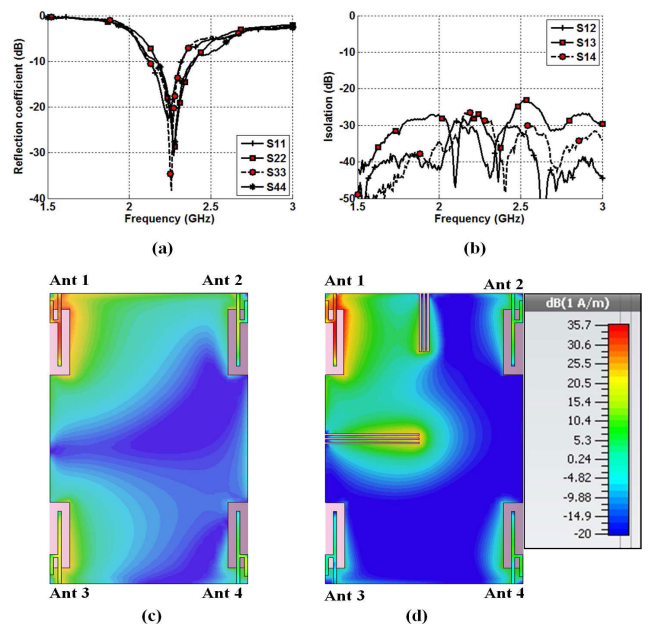
isolation of 30 dB is achieved between Antenna 1 and 2 while 29 dB was achieved between Antenna 1 and 3. An isolation improvement of 12 dB was obtained on average. There was a slight reduction of 30 MHz in the frequency BW and the main reason in our opinion seems to be the blockage of mode 4. Figure 15(c) and 15(d) show the current distribution on the surface of the antenna in the presence and absence of the DGS when only Ant-1 is excited. A significant improvement is obtained in isolation.

B. MONOPOLE BASED MIMO DESIGN
We will extend our study now to the 4-element MIMO monopole design. We can observe from Figure 9 that only

modes 1 and 2 are contributing in the desired impedance BW while modes 3, 4, 5 and 6 are not contributing at all. From Figure 8 we can observe that mode 1 is not causing significant coupling between the antennas connected on the longitudinal or horizontal sides. Mode 2 is causing the coupling between the antennas connected on the horizontal side.

The total current on the surface of the antenna and chassis is shown in Figure 16. The total current seems to be a combination of modes 1 and 2 but mode 1 seems to be more dominant because if mode 2 was dominant then the current distribution will be uniform and secondly the position where we have applied sources are more likely to enforce the excitation of longitudinal modes (i.e mode 1).
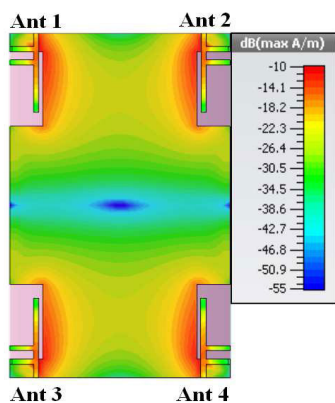

FIGURE 16. Current distribution on the surface of the 4-element MIMO monopole antenna and chassis at 2.2 GHz when all antennas are excited.

To enhance the isolation between Ant1 and Ant2, mode 2 seems to be the coupling mode, so it should be blocked but the position/location of the DGS should not affect mode 1 significantly. So we place the DGS at the horizontal center between Ant-1 and 2 as shown in Figure 7(b). It is the point where mode 1 has the current minima. The size of the DGS was optimized by having a length of 21 mm, width of the slit was 0.7 mm while separation was 1 mm. The total size of the DGS was 21×4.1 mm^2.

The CM current distribution at 2.2 GHz and the MS plots after introducing the DGS are shown in Figure 17 and 18, respectively. The CM current distribution of mode 2 is significantly affected and the DGS is producing currents in the direction opposite to the direction of mode 2 flow. Although mode 2 is blocked, it still appears in the middle of the impedance BW. But due to the current opposition by the DGS, even if it is present in the radiating BW region it will not be excited effectively. Since the addition of a DGS affects the geometry, now another mode is contributing in the band of interest i.e mode 3.

The reflection and isolation curves of the 4-element monopole design with DGS are shown in Figure 19(a) and 19(b) respectively. We can observe an improvement of 14.5 dB in the measured isolation between Ant-1 and 2 (S_{12}). Figure 19(c) and 19(d) show the current distribution on the surface of the antenna with and without
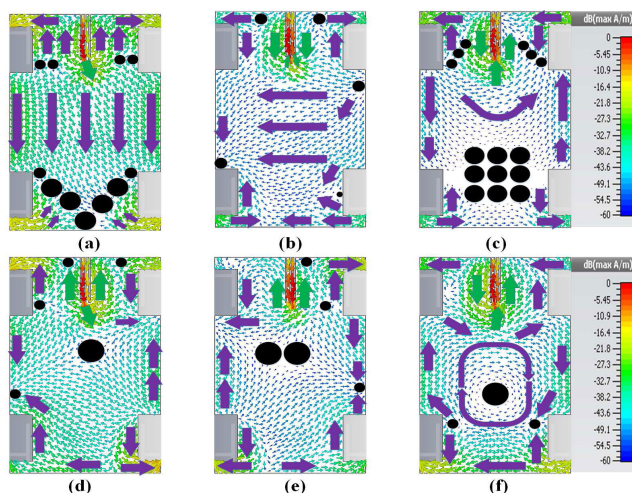

FIGURE 17. Current distribution of the first six modes of the 4-element Monopole based MIMO in the presence of DGS at 2.20 GHz, where (a) mode 1 (b) mode 2 (c) mode 3 (d) mode 4 (e) mode 5 (f) mode 6. The green arrows show the current distribution created due to the introduction of DGS. The black dots show the current null or current minima location while the violet arrows represent the current distribution on the surface of chassis.
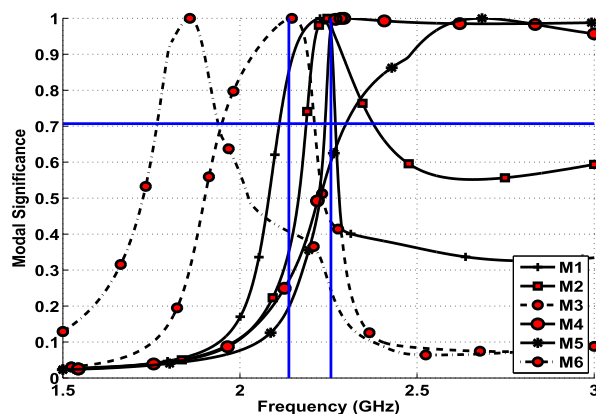

FIGURE 18. Modal significance curves of the 4-element MIMO Monopole in the presence of FR-4 substrate in the presence of DGS. The vertical blue lines represent the impedance BW.

DGS when Ant-1 is excited. A significant isolation improvement is obtained.

The second objective is to improve the isolation between the antennas connected on the longitudinal side. From the MS plot and the impedance BW in Figures 18 and 19(a), Mode 1 and the impedance BW nearly have the same radiating and impedance BW. That is mode 1 radiation BW is from 2.112 to 2.265 GHz while the impedance BW is from 2.138 to 2.257 GHz. Mode 3 is contributing from 1.952 to 2.209 GHz. Mode 3 decays in the middle of the impedance BW. From these two observations we can conclude that mode 1 is the non-coupling mode and mode 3 is the coupling mode.

To enhance the isolation, we need to block mode 3. But the current patterns on the edge and side of the chassis are nearly the same for both modes. Mode 1 has a current null
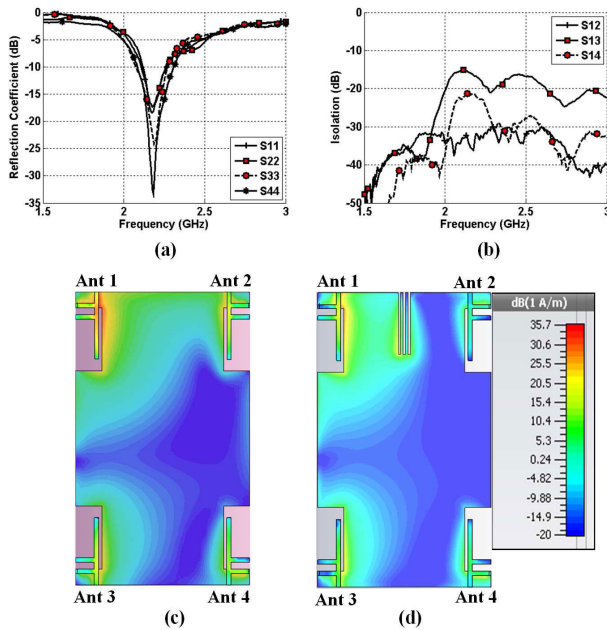
FIGURE 19. 4-element Monopole design, (a) measured reflection coefficient with DGS, (b) measured isolation curve with DGS, (c) current distribution without DGS when Ant-1 is excited, (d) current distribution with DGS when Ant-1 is excited.

FIGURE 20. 2-element wire monopole design, (a) reflection coefficient, (b) coupling coefficient, (c) modal significance curves of the 2-element MIMO wire monopole (mo DGS), and (d) modal significance curves of the 2-element MIMO wire monopole in the presence of DGS.

nearly at the same location as mode 3 so placing a slot at this location will create two problems. First, it will not meet the purpose because the slot will not affect the coupling mode significantly and second, placing a slot at such a location is not a realistic because it can completely isolate the antennas. The other strategy to improve the isolation will be to place the slot at such a location that it affects the coupling mode significantly while non-coupling mode is affected less severely. The optimum position seems to be the center of the chassis, but we cannot place the slot at the center of the chassis again due to two reasons. First, mode 1 current distribution seems stronger as compared to mode 3 (Figure 17) at the center so it will greatly affect mode 1 and will thus affect the impedance BW. Second, mode 1 radiating BW is very limited and introducing any discontinuity in the path will severely affect it. In such scenarios, using a DGS for isolation enhancement cannot be used and will not provide the improvement anticipated. We tried several parametric studies but we were not able to improve the isolation, thus it verified our conclusion.

C. WIRE MONOPOLE 2-ELEMENT MIMO DESIGN

A Wire Monopole antenna of length 32.5 mm and wire diameter of 1 mm was placed on a ground plane of 40×25 mm^2 size [20]. The center to center separation between the two antennas is $0.093\lambda_o$. The antennas are resonating with an impedance BW covering $2.2 - 2.45$ GHz while the isolation between the two antenna elements was 5.5 dB at 2.2 GHz as shown in Figure 20(a) and 20(b) respectively. To enhance the isolation, our proposed method was used, and for brevity purposes only the MS curves are shown in Figure 20(c).
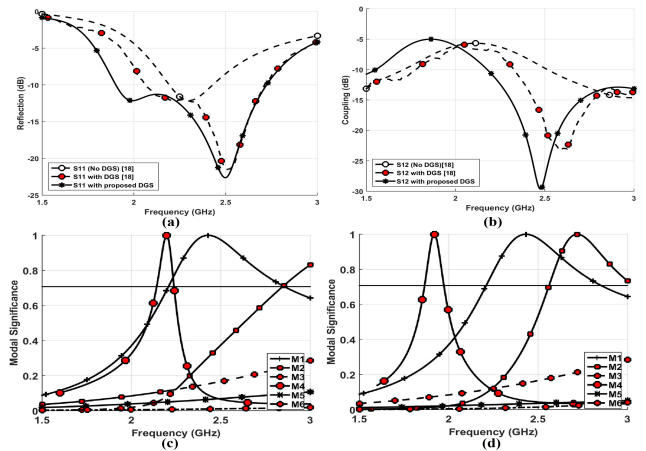
In our desired impedance BW region only two modes are contributing to the radiating BW they are mode 1 and 4. Mode 1 is having a current null between the antennas while mode 4 current was coupling the antennas. So, mode 1 is a non-coupling mode while mode 4 is a coupling mode. To block mode 4, we introduce a slitted DGS at the current null location of mode 1. The addition of the DGS significantly improved the isolation as shown in Figure 20(b) and mode 4 is no longer contributing in the desired BW as shown in Figure 20(d). We can observe a 20 dB improvement in the isolation at 2.45 GHz while in the BW of interest (the BW which we have initially from Figure 20(a) is 2.2 GHz to 2.45 GHz) the minimum isolation was 12.5 dB, which represents a 7-dB improvement. Comparing the isolation improvement using our method to the isolation improvement in [18], we observe that at 2.2 GHz the improvement in isolation is only 2.5 dB in [20], and it is not meeting the impedance matching criteria (VSWR<2.0) at 2.2 GHz (frequency shift) while in our case it is 12.5 dB and thus it is meeting the criteria.

D. SUMMARY

In the above sections we have provided a physical explanation to the operation of a DGS with the help of TCM, as well we have proposed a method that can directly help the designer use such structures in a systematic way and in identifying whether isolation can be improved or not.

The Block diagram of the proposed method is shown in Figure 21. After analyzing three different designs we developed steps for improving the isolation between antenna elements of monopole or PIFA like structures. For the system under consideration, first we need to perform TCM analysis to identify the modes present in the band of interest. Then we need to check the current patterns on the surface of the antenna and identify coupling and non-coupling modes visually. Based on the current patterns, the DGS shall be placed at certain locations so that the non-coupling modes

TABLE 1. Isolation enhancement comparison with previous works.

References	No. Of Ant.	Antenna Type	No. of Isol.	Isolation method	Antenna Size (mm^2)	DGS size (mm^2)	Operating bands (GHz)	Without DGS. Isol.(dB)	Worst DGS isol. (dB)	Improv. across band (dB)
[14]	2	Patch	1	DGS	-	16×20.76	2.57	15	23	5
[15]	2	Slot	2	DGS	22×26	-	3.1-10.6	8	18	10
[16]	2	Patch	1	DGS	60.2×60.2	38×38	2.45	18	25	7
[17]	2	4 shaped	1	DGS	100×50	52×11	0.803-0.823 & 2.44-2.9	-	17 & 9	-
[18]	2	L-slot	2	DGS + Orth.Placement	32×32	13×1	3-4.5	11.5	15	3.5
[19]	4	Cylindrical Monopole	3	DGS + MO-FFD	$\pi \times 80^2 \times 50$	-	0.698-0.960	10	12 & 18	2 & 6
[20]	2	PIFA	1	DGS	43×43	21×9	2.27-2.35	12.5	20	7.5
	2	Wire Monopole	1	DGS	40×25	5×25	2.2-2.45	5.5	8.0	2.5
	3	PIFA	1	DGS	103×43	21×9	-	-	12	-
	4	PIFA	1	DGS	143×43	21×9	-	-	12	-
[21]	4	F-shaped	2	DGS	120×60	120×47	Reconfig.	9	12.5	3
[22]	4	PIFA	1	DGS	100×60	28.5×2.5	2.07-2.21	15 & 10	15 & 15	0 & 5
[23]	4	Monopole	1	DGS	100×60	35×10.5 & $\pi(9)^2$	2.02-2.205	15 & 15	15 & 20	0 & 5
[24]	8	Ring slot	3	DGS+CL-FSS+Arcs	93×60	93×60	4.0-10	-	15 & 20	-
Proposed Method	4	PIFA [22]	1	DGS	100×60	28.5×3.5,20×4.5	2.17-2.33	16.25 & 18.5	29 & 30	12.75 & 11.5
	4	Monopole [23]	1	DGS	100×60	21×4.1	2.13-2.26	15.5 & 17.3	17.5 & 32.8	14.5
	2	Monopole [20]	1	DGS	40×25	3.7×25	2.2-2.45	5.5	12.5	7
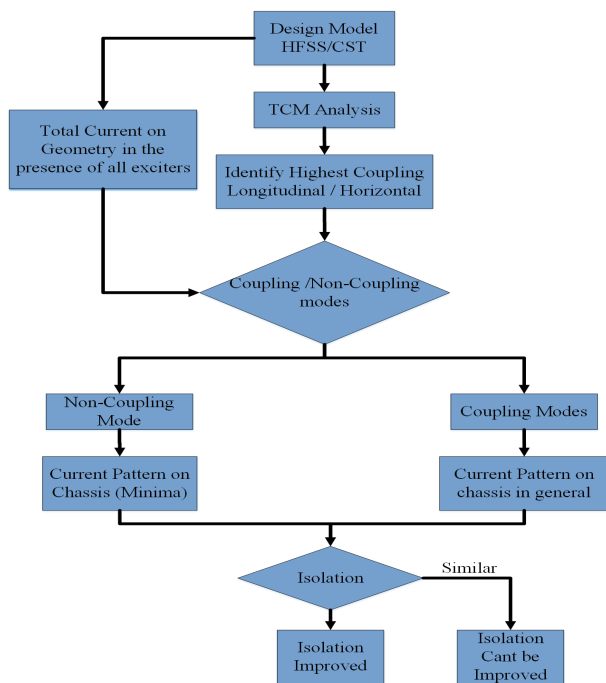
FIGURE 21. Block diagram of the proposed isolation enhanced TCM based method using DGS.

appeared in literature. Table 1 shows that our proposed scheme is providing the highest isolation improvement and at the same time is the lowest in complexity and more generalized as compared to other methods. In other techniques, we need to apply several methods and parametric studies but still we are not sure whether the system can provide the desired isolation. In the proposed TCM based systematic method just by studying the first few modes we can deduce for a particular system, whether isolation can be achieved or not.

For isolation enhancement most of the works have focused on 2-element designs and listed the isolation at the best point. In case of [20] the 3 and 4 elements are placed on one axis (not in rectangular or square fashion), so its the same as a 2 element design extended in one axis. We have achieved the highest improvement in the isolation for the whole impedance BW with a relatively small DGS size. The improvement in isolation between Ant1 and Ant3 does not guarantee isolation improvement between Ant2 and Ant4. But to improve the isolation between Ant2 and Ant4, the same DGS (with little modification) shall be also placed between Ant 2 and 4. This is the shortcoming of DGS approach in general. Here our focus was to develop a systematic approach with the help of TCM and verify its effectiveness.

IV. MIMO ANTENNA PARAMETER EVALUATION
MIMO antenna systems shall be evaluated for parameters such as Envelope correlation coefficient (ECC), Gain, efficiency and 2D/3D radiation patterns. ECC (ρ_e) values are computed using the 3D measured radiation patterns in an isotropic multi-path environment [1]:

are unaffected while the coupling modes are blocked. After observing the CM current distribution, if there is no such point on the chassis or the current pattern of the coupling and non-coupling modes is almost same on the chassis, then isolation cannot be enhanced further.

Isolation enhancement that was achieved by our proposed TCM based method was compared against the isolation achieved by other specific DGS based structures that

$$\rho_e = \frac{|\int\int_{4\pi}[\vec{F}_1(\theta, \varphi) * \vec{F}_2(\theta, \varphi)d\Omega]|^2}{|\int\int_{4\pi}[\vec{F}_1(\theta, \varphi)|^2 d\Omega \int\int_{4\pi}[\vec{F}_2(\theta, \varphi)|^2 d\Omega} \quad (4)$$
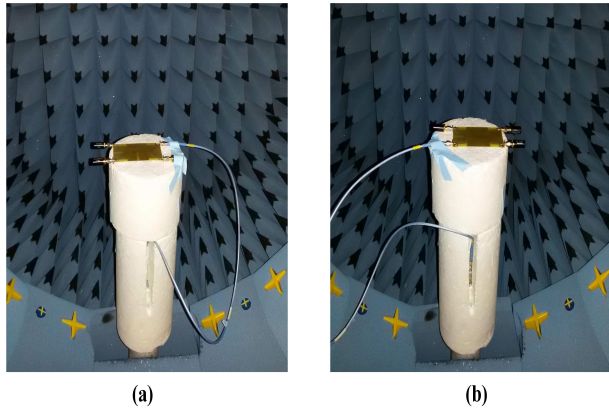
FIGURE 22. Radiation pattern measurement setup (a) 4-element MIMO PIFA (b) 4-element MIMO Monopole.

FIGURE 24. Measured Gain and efficiency curves for (a) 4-element MIMO PIFA, (b) 4-element MIMO Monopole.

TABLE 2. Measured ECC(ρ_e). all frequencies are in GHz.

Freq (GHz)	ρ_{e12}	ρ_{e13}	ρ_{e14}	ρ_{e23}	ρ_{e24}	ρ_{e34}
2.20	0.175	0.040	0.041	0.012	0.123	0.132
2.22	0.165	0.037	0.040	0.013	0.134	0.122
2.24	0.160	0.033	0.039	0.014	0.146	0.116
2.26	0.160	0.028	0.038	0.015	0.159	0.113

where $\vec{F}_i(\theta, \varphi)$ is the field radiation pattern of the antenna when port i is excited and $*$ denotes the Hermitian product. For the given MIMO antenna systems, ECC was calculated at four distinct frequencies for the printed designs. The gain pattern and efficiency measurement setup is shown in Figure 22. The gain pattern of an individual antenna element was obtained while the other ports were terminated with 50 Ω loads.

FIGURE 25. Monopole-based MIMO antenna measured and simulated normalized radiation patterns at 2.20 GHz (Etotal) (a) (ϕ cut) Ant 1 and 2 at $\theta = 90$, (b) (θ cut) Ant 1 and 2 at $\phi = 0$,(c) (ϕ cut) Ant 3 and 4 at $\theta = 90$, (b) (θ cut) Ant 3 and 4 at $\phi = 0$.

TABLE 3. Measured ECC(ρ_e) . all frequencies are in GHz.

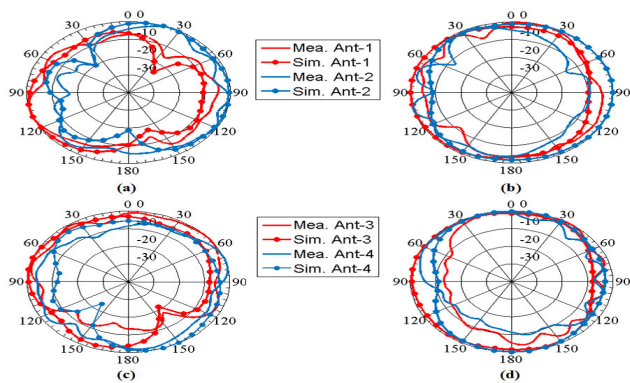| Freq (GHz)	ρ_{e12}	ρ_{e13}	ρ_{e14}	ρ_{e23}	ρ_{e24}	ρ_{e34}
2.20	0.193	0.098	0.068	0.029	0.126	0.256
2.22	0.203	0.109	0.075	0.033	0.135	0.250
2.24	0.211	0.118	0.083	0.036	0.143	0.246
2.26	0.216	0.124	0.091	0.036	0.149	0.244

FIGURE 23. PIFA-based MIMO antenna measured and simulated normalized radiation patterns at 2.20 GHz (Etotal) (a) (ϕ cut) Ant 1 and 2 at $\theta = 90$, (b) (θ cut) Ant 1 and 2 at $\phi = 90$,(c) (ϕ cut) Ant 3 and 4 at $\theta = 90$, (b) (θ cut) Ant 3 and 4 at $\phi = 90$.

A. PIFA BASED MIMO DESIGN

The simulated and measured normalized 2D radiation patterns in terms of the total E-field (Etotal) at 2.20 GHz are shown in Figure 23. The patterns show the x-y and y-z planes for all the antenna elements. Good agreement is obtained between the simulated and measured results. The measured gain and efficiency curves for Ant1 are shown in the Figure 24(a) (other elements have similar values). The measured highest gain of 6.45 dB was obtained with an efficiency of around 97 % at 2.257 GHz. ECC values are shown in the Table 2. We can observe that the worst ECC value is 0.175 which is far below the threshold value of 0.5.
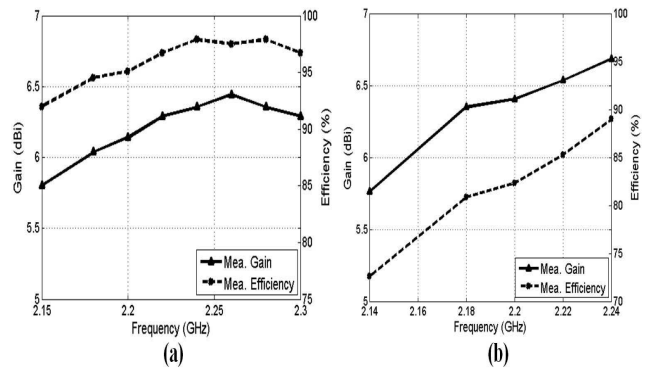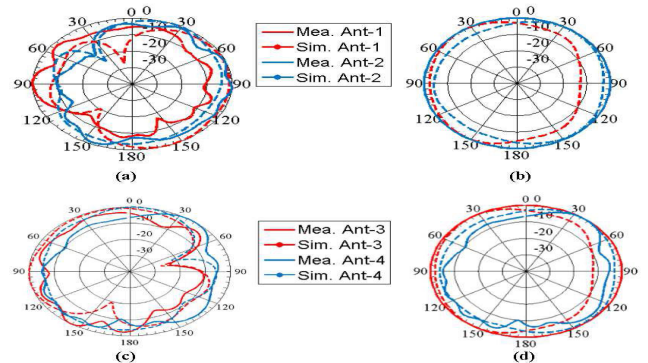
B. MONOPOLE BASED MIMO DESIGN

The simulated and measured normalized 2D radiation patterns in terms of the total E-field (Etotal), at 2.20 GHz are shown in Figure 25. The patterns show the x-y and x-z planes for all the antenna elements. Good agreement is obtained between the simulated and measured results. Measured gain and efficiency curves for Ant1 are shown in the Figure 24(b). The measured highest gain of 6.55 dB was obtained with an efficiency of around 89 % at 2.24 GHz. ECC values are

shown in the Table 3. We can observe that the worst ECC value is 0.256.

V. CONCLUSIONS

In this paper, TCM was used to analyze the behavior as well as develop a systematic approach for the placement of DGS in MIMO antenna configurations. We considered one 2-element wire and two 4-element printed MIMO antenna designs in the analysis. The presence of PIFA and Monopole antennas significantly affect the CM and MS curves. The developed approach was applied to all designs and an average isolation enhancement of almost 11 dB was achieved. The method is compared to the already published approaches in which isolation was achieved by DGS and any other schemes. Our proposed method is simple, achieved more isolation and can be generalized to different antenna designs. The two MIMO antennas, PIFA and Monopole were fully characterized and showed efficiency values higher than 85 % and 75 % and ECC lower then 0.175 and 0.256 respectively. All the analysis included the effect of the dielectric substrate. Very good agreement between simulated and measured results is obtained.

REFERENCES

[1] M. S. Sharawi, *Printed MIMO Antenna Engineering*. Norwood, MA, USA: Artech House, 2014.

[2] G. Zhai, Z. N. Chen, and X. Qing, "Enhanced isolation of a closely spaced four-element mimo antenna system using metamaterial mushroom," *IEEE Trans. Antennas Propag.*, vol. 63, no. 8, pp. 3362–3370, Aug. 2015.

[3] D. K. Ntaikos and T. V. Yioultsis, "Compact split-ring resonator-loaded multiple-input-multiple-output antenna with electrically small elements and reduced mutual coupling," *IET Microw., Antennas Propag.*, vol. 7, no. 4, pp. 421–429, Apr. 2013.

[4] C. C. Hsu, K. H. Lin, and H. L. Su, "Implementation of broadband isolator using metamaterial-inspired resonators and a T-shaped branch for MIMO antennas," *IEEE Trans. Antennas Propag.*, vol. 59, no. 10, pp. 3936–3939, Oct. 2011.

[5] C.-Y. Lui, Y.-S. Wang, and S.-J. Chung, "Two nearby dual-band antennas with high port isolation," in *Proc. IEEE Antennas Propag. Soc. Int. Symp.*, Jul. 2008, pp. 1–4.

[6] Y. Wang and Z. Du, "A wideband printed dual-antenna with three neutralization lines for mobile terminals," *IEEE Trans. Antennas Propag.*, vol. 62, no. 3, pp. 1495–1500, Mar. 2014.

[7] A. Diallo, C. Luxey, P. L. Thuc, R. Staraj, and G. Kossiavas, "Study and reduction of the mutual coupling between two mobile phone PIFAs operating in the DCS1800 and UMTS bands," *IEEE Trans. Antennas Propag.*, vol. 54, no. 11, pp. 3063–3074, Nov. 2006.

[8] S. Soltani and R. D. Murch, "A compact planar printed MIMO antenna design," *IEEE Trans. Antennas Propag.*, vol. 63, no. 3, pp. 1140–1149, Mar. 2015.

[9] A. C. K. Mak, C. R. Rowell, and R. D. Murch, "Isolation enhancement between two closely packed antennas," *IEEE Trans. Antennas Propag.*, vol. 56, no. 11, pp. 3411–3419, Nov. 2008.

[10] R. R. Ramirez and F. D. Flaviis, "A mutual coupling study of linear and circular polarized microstrip antennas for diversity wireless systems," *IEEE Trans. Antennas Propag.*, vol. 51, no. 2, pp. 238–248, Feb. 2003.

[11] B. Wu and K. M. Luk, "A 4-port diversity antenna with high isolation for mobile communications," *IEEE Trans. Antennas Propag.*, vol. 59, no. 5, pp. 1660–1667, May 2011.

[12] H. Kim and S. Kahng, "Design of a compact four MIMO handset antenna structure," *Microw. J.*, vol. 59, no. 4, pp. 162–174, 2016.

[13] S. Kahng, J. Jeon, J. Anguera, and T. Park, "A compact MIMO antenna using CRLH configuration double-layered folded ring radiations with planar mushroom decoupling structure," *IEEE Antennas Propag. Mag.*, vol. 57, no. 4, pp. 123–130, Apr. 2015.

[14] K. Wei, J. Li, L. Wang, Z. Xing, and R. Xu, "S-shaped periodic defected ground structures to reduce microstrip antenna array mutual coupling," *Electron. Lett.*, vol. 52, no. 15, pp. 1288–1290, Jul. 2016.

[15] C. M. Luo, J. S. Hong, and L. L. Zhong, "Isolation enhancement of a very compact uwb-mimo slot antenna with two defected ground structures," *IEEE Antennas Wireless Propag. Lett.*, vol. 14, pp. 1766–1769, 2015.

[16] R. Anitha, V. P. Sarin, P. Mohanan, and K. Vasudevan, "Enhanced isolation with defected ground structure in MIMO antenna," *Electron. Lett.*, vol. 50, no. 24, pp. 1784–1786, Dec. 2014.

[17] M. S. Sharawi, A. B. Numan, M. U. Khan, and D. N. Aloi, "A dual-element dual-band MIMO antenna system with enhanced isolation for mobile terminals," *IEEE Antennas Wireless Propag. Lett.*, vol. 11, pp. 1006–1009, 2012.

[18] J. Ren, W. Hu, Y. Yin, and R. Fan, "Compact printed MIMO antenna for UWB applications," *IEEE Antennas Wireless Propag. Lett.*, vol. 13, pp. 1517–1520, 2014.

[19] Y. S. Chen and C. P. Chang, "Design of a four-element multiple-input-multiple-output antenna for compact long-term evolution small-cell base stations," *IET Microw., Antennas Propag.*, vol. 10, no. 4, pp. 385–392, Apr. 2016.

[20] C. Y. Chiu, C. H. Cheng, R. D. Murch, and C. R. Rowell, "Reduction of Mutual Coupling Between Closely-Packed Antenna Elements," *IEEE Trans. Antennas Propag.*, vol. 55, no. 6, pp. 1732–1738, Jun. 2007.

[21] R. Hussain and M. S. Sharawi, "Planar meandered-f-shaped 4-element reconfigurable multiple-input-multiple-output antenna system with isolation enhancement for cognitive radio platforms," *IET Microw., Antennas Propag.*, vol. 10, no. 1, pp. 45–52, Jan. 2016.

[22] M. Ikram, R. Hussain, A. Ghalib, and M. S. Sharawi, "Compact 4-element MIMO antenna with isolation enhancement for 4G LTE terminals," in *Proc. IEEE Int. Symp. Antennas Propag. (APSURSI)*, Jun. 2016, pp. 535–536.

[23] M. Ikram, R. Hussain, O. Hammi, and M. S. Sharawi, "An l-shaped 4-element monopole mimo antenna system with enhanced isolation for mobile applications," *Microw. Opt. Technol. Lett.*, vol. 58, no. 11, pp. 2587–2591, Nov. 2016.

[24] R. Saleem, M. Bilal, K. B. Bajwa, and M. F. Shafique, "Eight-element UWB-MIMO array with three distinct isolation mechanisms," *Electron. Lett.*, vol. 51, no. 4, pp. 311–313, Apr. 2015.

[25] R. J. Garbacz, "A generalized expansion for radiated scattered fields," Ph.D. dissertation, Elect. Eng. Dept., Ohio State Univ., Columbus, OH, USA, 1968.

[26] R. F. Harrington and J. R. Mautz, "Theory of characteristic modes for conducting bodies," *IEEE Trans. Antennas Propag.*, vol. 19, no. 5, pp. 622–628, Sep. 1971.

[27] M. C. Fabres, "Systematic design antennas using theory characteristic modes," Ph.D. dissertation, Elect. Eng. Dept., Polytech. Univ. Valencia, Valencia, Spain, Feb. 2007.

[28] E. Antonino, "Analysis and design of antennas for wireless communications using modal methods," Ph.D. dissertation, Elect. Eng. Dept., Polytech. Univ. Valencia, Valencia, Spain, Feb. 2008.

[29] H. Li, Z. T. Miers, and B. K. Lau, "Design of Orthogonal MIMO handset antennas based on characteristic mode manipulation at frequency bands below 1 GHz," *IEEE Trans. Antennas Propag.*, vol. 62, no. 5, pp. 2756–2766, May 2014.

[30] R. Martens, E. Safin, and D. Manteuffel, "Selective excitation of characteristic modes on small terminals," in *Proc. 5th Eur. Conf. Antennas Propag. (EUCAP)*, Apr. 2011, pp. 2492–2496.

[31] R. Martens and D. Manteuffel, "Systematic design method of a mobile multiple antenna system using the theory of characteristic modes," *IET Microw., Antennas Propag.*, vol. 8, no. 9, pp. 887–893, Sep. 2014.

[32] R. Martens, J. Holopainen, E. Safin, J. Ilvonen, and D. Manteuffel, "Optimal dual-antenna design in a small terminal multiantenna system," *IEEE Antennas Wireless Propag. Lett.*, vol. 12, pp. 1700–1703, 2013.

[33] H. Li, Y. Tan, B. K. Lau, Z. Ying, and S. He, "Characteristic mode based tradeoff analysis of antenna-chassis interactions for multiple antenna terminals," *IEEE Trans. Antennas Propag.*, vol. 60, no. 2, pp. 490–502, Feb. 2012.

[34] H. Li, B. K. Lau, Z. Ying, and S. He, "Decoupling of multiple antennas in terminals with chassis excitation using polarization diversity, angle diversity and current control," *IEEE Trans. Antennas Propag.*, vol. 60, no. 12, pp. 5947–5957, Dec. 2012.

ASIM GHALIB received B.Sc. and M.Sc. degrees in electrical engineering from the University of Engineering and Technology, Peshawar, Pakistan, in 2011 and 2014, respectively. He is currently pursuing the Ph.D. degree in electrical engineering with the King Fahd University of Petroleum and Minerals, Dhahran, Saudi Arabia.

His research interests include design and analysis of MIMO antennas based on the theory of characteristic modes.

MOHAMMAD S. SHARAWI (SM'10) was born in Wolfsburg, Germany, in 1977. He received the B.Sc. degree in electronics engineering degree (Hons.) from the Princess Sumaya University for Technology, Amman, Jordan, in 2000, the M.Sc. degree in electrical and computer engineering and the Ph.D. degree in RF systems engineering from Oakland University, Rochester, Michigan, USA, in 2002 and 2006, respectively, with a focus on Microwave and Antenna Systems Design. He was a Visiting Associate Professor with the Intelligent Radio Laboratory, Electrical Engineering Department, University of Calgary, AB, Canada, in 2014. He was a Visiting Research Professor, Oakland University, in 2013. In 2009, he was a Research Scientist with the Applied Electromagnetics and Wireless Laboratory, Electrical and Computer Engineering Department, Oakland University, Michigan, USA, from 2008 to 2009. He was a Faculty Member with the Computer Engineering Department, Philadelphia University, Amman, Jordan, from 2007 to 2008 He was the acting Head of the Computer Engineering, Department, German-Jordanian University, Amman, Jordan from 2006 to 2007. He is currently a Professor in electrical engineering with the King Fahd University of Petroleum and Minerals (KFUPM), Dhahran, Saudi Arabia. He has authored over 200 refereed journal and conference papers and has 12 issued and 14 pending patents with the USPO. He is the single author of the book *P*rinted MIMO Antenna Engineering, (Artech House, 2014), and the Lead Author of *D*esign and Applications of Active Integrated Antennas, (Artech House, 2018). His research interests include printed antennas and antenna arrays, mimo antenna systems, millimeter-wave antennas, reconfigurable antennas, applied electromagnetics, microwave electronics, and microwave system integration. He served as the Organization Committee Chair of the IEEE Conference on Systems, Signals, and Devices that was held in Jordan 2008. He was an exchange student during the academic year of with the University of Illinois at Urbana–Champaign in 1997 and 1998. He was an Intern with Silicon Graphics Inc (SGI), Mountain View, California, USA, in 1998, 2001, and 2002, where he was involved various circuits design and interconnect modeling projects.

Prof. Sharawi was a Member of Technical Staff Design Engineer with SGI from 2002 to 2003, where he was responsible for modeling, design, and verification of high speed PCBs and circuits for various high performance computing systems. He is the founder and director of the Antennas and Microwave Structure Design Laboratory, KFUPM. He has received over 10 Million SAR in research funding 2.5 Million USD in 7 years, while with KFUPM. He has organized several special sessions in International IEEE conferences in the area of Printed, MIMO, and Millimeter-wave antenna systems and served on the technical program committees at APS, EuCAP, APCAP, ICCE, and APWC among other international conferences.

• • •